UC San Diego
UC San Diego Electronic Theses and Dissertations

Title
Helical Contour Dynamics

Permalink
https://escholarship.org/uc/item/3ng4s8vk

Author
Chu, Tianyi

Publication Date
2018

Peer reviewed|Thesis/dissertation

eScholarship.org Powered by the California Digital Library
University of California

UNIVERSITY OF CALIFORNIA SAN DIEGO

Helical Contour Dynamics

A thesis submitted in partial satisfaction of the
requirements for the degree
Master of Science

in

Engineering Sciences (Mechanical Engineering)

by

Tianyi Chu

Committee in charge:

Professor Stefan G. Llewellyn Smith, Chair
Professor Antonio L. Sanchez
Professor Oliver T. Schmidt

2018

Copyright
Tianyi Chu, 2018
All rights reserved.

The thesis of Tianyi Chu is approved, and it is acceptable in quality and form for publication on microfilm and electronically:

Chair

University of California San Diego

2018

TABLE OF CONTENTS

LIST OF FIGURES

ACKNOWLEDGEMENTS

I would like to acknowledge Professor Stefan G. Llewellyn Smith for his support as the chair of my committee. Although he was very busy, he spent a lot of time meeting with me. He took me under his wing, saw the potential in this project and gave for insightful guidance.

I would also like to acknowledge Ching Chang who gave me a lot of valuable advice for my thesis. Without him my research would no doubt take much longer. His support that helped me in an immeasurable way.

The thesis is currently being prepared for submission for publication of the material. Tianyi Chu, Stefan G. Llewellyn Smith and Ching Chang. The thesis author was the primary investigator and author of this material.

ABSTRACT OF THE THESIS

Helical Contour Dynamics

by

Tianyi Chu

Master of Science in Engineering Sciences (Mechanical Engineering)

University of California San Diego, 2018

Professor Stefan G. Llewellyn Smith, Chair

In an incompressible inviscid flow system, helical symmetry means invariance though combined axial translation and rotation about the same axis. In helical symmetry, the axial vorticity is materially conserved if the velocity components along the helical lines are proportional to $(1+\varepsilon^2 r^2)^{-1}$, where ε is the pitch and r is the distance from the z axis. Linear instability analysis shows that a circular helical vortex patch centered at the origin is neutrally stable. We present the evolution of a family of helically symmetric vortices using contour dynamics, a Lagrangian technique to compute the motion of vortices via contour integrals. For contours perturbed by both lower and high modes, the first mode always becomes the most unstable mode for large time. We can inspect the features induced by the lower perturbed mode. We take mode 4 and mode 9 as

examples in this work. Adding a vortex sheet on the boundary of the shifted contour accelerates the twisting and rotating process. The distribution of vortex sheet forms a sharpening shock in the evolution and may lead to the discontinuity.

Chapter 1

Introduction

Helical vortices are commonly found in the wake of rotating bladed devices such as marine propellers, wind turbines, or helicopters [S.V. ALEKSEENKO & S.I.SHTORK(1999)]. Within a certain downstream distance of the rotating device, the flow system can be considered as locally helical symmetric, which means that it is locally invariant through combined translation and rotation about the same axis. With this assumption, previous works have studied the time evolution of viscous helical vortices. [DELBENDE(2012)] simulated the viscous dynamics of several helical vortices and presented quasi-steady states using a DNS method. [SELÇUK *et al.*(2017)SELÇUK, DELBENDE & ROSSI] described characterizes of helical quasi-equilibrium states as a function of helix radius, angular velocity, stream function, and core properties. Recent studies have also examined the linear stability of a helical vortices. [WIDNALL(1972)] initially considered the linear stability of a vortex filament of finite core by obtaining the self-induced motion due to small sinusoidal displacements. [LUCAS & DRITSCHEL(2009)] used helical symmetry to compute equilibria of helical vortices with arbitrary sizes and constant pitch in a rotating frame of reference. For such helically symmetric flows with a particular choice of the velocity component parallel to vortex lines, the axial vorticity is materially conserved in an absolute frame of reference. The class of equilibria is parametrized by mean core radius and also by centroid position. Each equilibrium state consists of a single closed contour bounding a uniform distribution of vorticity. [HATTORI & FUKUMOTO(2014)] investigated the linear stability of a helical vortex tube with axial flow. They expanded the linearized incompressible Euler equations in the ratio of the core to curvature radius of the tube. The unstable growth rate can be evaluated using the Kelvin waves with the expanded equations.

In this work, we examine the time evolution of inviscid helical vortex with helical symmetry through contour dynamics methods. This approach reduces the evolution of vortex patches to the evolution of the boundary and thus the dimensionality of the system. Similar to [LUCAS & DRITSCHEL(2009)], we take the vorticity as well as the velocity component parallel to vortex lines to be piecewise constant, and allow a vortex sheet to develop on the boundary. From the stream function-vorticity relation in helical coordinates, we can compute velocities by inverting a linear helical operator $\mathscr{L}\psi$ analytically. The two main problems posed by our approach are in finding an appropriate Green's function for the system and obtaining the equations for contour dynamics. The linear instability analysis is presented to compare with the result from contour dynamics.

Chapter 2

Helical Symmetric Flow

Consider an inviscid and incompressible flow which has helical symmetry , which means that the velocity, vorticity and pressure fields are invariant with respect to the helical vector $\boldsymbol{h}$ [DRITSCHEL(1991)]. In cylindrical coordinates (r, θ, z), $\boldsymbol{h}$ is given by

$$\boldsymbol{h} = h^2 \left(\boldsymbol{e}_z - \varepsilon r \boldsymbol{e}_\theta \right), \tag{2.1}$$

where $h^2 = (1 + \varepsilon^2 r^2)^{-1}$ and ε is the pitch of the helix. Note that $/boldsymbolh$ is not a unit vector here. Helical symmetry also implies that $\boldsymbol{h} \cdot \nabla = 0$ for any scalar functions of r, ϕ and t, where $\phi = \theta + \varepsilon z$ is the helical coordinate. When $\varepsilon = 0$, the flow becomes two-dimensional, while $\varepsilon = \infty$ represents the axisymmetric case. The unit vector for the helical coordinate ϕ is defined by

$$\boldsymbol{e}_\phi = h^{-1} \boldsymbol{h} \times \boldsymbol{e}_r = h \left(\boldsymbol{e}_\theta + \varepsilon r \boldsymbol{e}_z \right). \tag{2.2}$$

In helical coordinates, the gradient operator becomes

$$\nabla = \boldsymbol{e}_r \frac{\partial}{\partial r} + \boldsymbol{e}_\theta \frac{1}{r} \frac{\partial}{\partial \theta} + \boldsymbol{e}_z \frac{\partial}{\partial z} = \boldsymbol{e}_r \frac{\partial}{\partial r} + (h \boldsymbol{e}_\phi - \varepsilon r \boldsymbol{h}) \frac{1}{r} \frac{\partial}{\partial \phi} + \varepsilon (\mathbf{h} + \varepsilon r h \boldsymbol{e}_\phi) \frac{\partial}{\partial \phi} = \boldsymbol{e}_r \frac{\partial}{\partial r} + \boldsymbol{e}_\phi \frac{1}{rh} \frac{\partial}{\partial \phi}.$$

A schematic of the helical coordinate system is shown in figure 2.1.

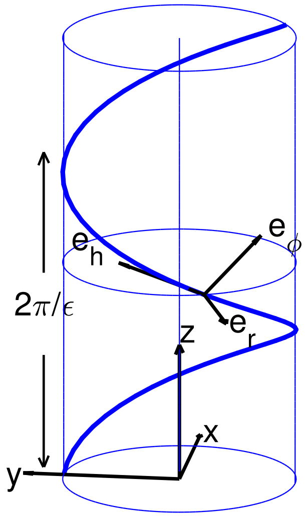

Figure 2.1: Schematic of the helical coordinate system. The axial distance between successive twists is $2\pi/\varepsilon$. Note that the vectors $\boldsymbol{h}$ and $\boldsymbol{e}_\phi$ lie on the surface of the cylinder $r =$constant. The special case we considered in this work is that the vorticity $\boldsymbol{\omega}$ is everywhere tangent to $\boldsymbol{h}$.

In order for the velocity and vorticity to be divergence free, we have the following decomposition in terms of helical scalar functions:

$$\boldsymbol{u} = \boldsymbol{h} \times \nabla\psi + \boldsymbol{h} v, \tag{2.3}$$

$$\boldsymbol{\omega} = \boldsymbol{h} \times \nabla\chi + \boldsymbol{h}\zeta. \tag{2.4}$$

The quantities ψ and v only depend on r and ϕ. From this decomposition, the velocity components in cylindrical coordinate systems are given by

$$u_r = -\frac{1}{r}\frac{\partial\psi}{\partial\phi}, \qquad u_\theta = h^2\left(\frac{\partial\psi}{\partial r} - \varepsilon r v\right), \qquad u_z = h^2\left(v + \varepsilon r\frac{\partial\psi}{\partial r}\right). \tag{2.5}$$

In helical coordinates, we have

$$u_r = -\frac{1}{r}\frac{\partial \psi}{\partial \phi}, \quad u_\phi = h\frac{\partial \psi}{\partial r}, \quad u_h = v. \tag{2.6}$$

From to the definition of vorticity $\boldsymbol{\omega} = \nabla \times \boldsymbol{u}$, consider the term $\omega = \boldsymbol{h} \cdot \boldsymbol{\omega}$. We have

$$\begin{aligned}\omega = \mathbf{h} \cdot (\nabla \times \mathbf{u}) = \mathbf{h} \cdot [\nabla \times (\mathbf{h} \times \nabla \psi + \mathbf{h} v)] &= -2\varepsilon h^2 \mathbf{h} \cdot (\mathbf{h} \times \nabla \psi) - \nabla \cdot \left[h^2 \nabla \psi\right] - 2\varepsilon h^4 v \\ &= \frac{1}{r}\frac{\partial}{\partial r}\left(r h^2 \frac{\partial \psi}{\partial r}\right) + \frac{1}{r^2}\frac{\partial \psi}{\partial \phi} - 2\varepsilon h^4 v.\end{aligned}$$

The equation coupling vorticity and stream function becomes [DRITSCHEL(1991)]:

$$\mathscr{L}\psi = \frac{1}{r}\frac{\partial}{\partial r}\left(r h^2 \frac{\partial \psi}{\partial r}\right) + \frac{1}{r^2}\frac{\partial \psi}{\partial \phi} = \omega + 2\varepsilon h^4 v. \tag{2.7}$$

From the inviscid Navier-Stokes and vorticity equation, we have

$$\begin{aligned}&\frac{\partial \boldsymbol{u}}{\partial t} + \boldsymbol{\omega} \times \boldsymbol{u} = -\nabla\left(\frac{P}{\rho} + \frac{1}{2}|\boldsymbol{u}|^2\right), \\ &\frac{\partial \boldsymbol{u}}{\partial t} + \nabla \times (\boldsymbol{\omega} \times \boldsymbol{u}) = 0.\end{aligned}$$

Taking the scalar product of both equations with $\boldsymbol{h}$, we obtain the following:

$$\begin{aligned}&\boldsymbol{h} \cdot \left(\frac{\partial \boldsymbol{u}}{\partial t} + \boldsymbol{\omega} \times \boldsymbol{u}\right) = \boldsymbol{h} \cdot \left[-\nabla\left(\frac{P}{\rho} + \frac{1}{2}|\boldsymbol{u}|^2\right)\right]. \\ \Rightarrow &\boldsymbol{h} \cdot \frac{\partial}{\partial t}(\boldsymbol{h} \times \nabla \psi + \boldsymbol{h} v) + [\boldsymbol{h} \times (-\boldsymbol{h} \times \nabla v + \boldsymbol{h}\zeta)] \cdot (\boldsymbol{h} \times \nabla \psi + \boldsymbol{h} v) = 0. \\ \Rightarrow &h^2\left(\frac{\partial v}{\partial t} + \boldsymbol{h} \cdot (\nabla \psi \times \nabla v)\right) = 0.\end{aligned}$$

$$
\begin{aligned}
&\mathbf{h}\cdot\left[\frac{\partial\boldsymbol{\omega}}{\partial t}+\nabla\times(\boldsymbol{\omega}\times\mathbf{u})\right]=0.\\
\Rightarrow&\mathbf{h}\cdot\frac{\partial}{\partial t}(-\mathbf{h}\times\nabla v+\mathbf{h}\zeta)+(\nabla\times\mathbf{h})\cdot(\boldsymbol{\omega}\times\mathbf{u})-\nabla\cdot[\mathbf{h}\times(\boldsymbol{\omega}\times\mathbf{u})]=0.\\
\Rightarrow&\frac{\partial\omega}{\partial t}-2\varepsilon h^4\boldsymbol{h}\cdot(\nabla\psi\times\nabla v)+2\varepsilon^2h^4v\frac{\partial v}{\partial\phi}+\boldsymbol{h}\cdot(\nabla\psi\times\nabla\omega)=0.
\end{aligned}
$$

By using the helical Jacobian $J(f,g)$ defined by

$$
J(f,g)=\frac{1}{r}\left(\frac{\partial f}{\partial r}\frac{\partial g}{\partial\phi}-\frac{\partial f}{\partial\phi}\frac{\partial g}{\partial r}\right)=\boldsymbol{h}\cdot(\nabla f\times\nabla g),
$$

the full nonlinear dynamical equations in an absolute frame [LUCAS & DRITSCHEL(2009)] can be obtained as

$$
\frac{\mathrm{D}v}{\mathrm{D}t}=\frac{\partial v}{\partial t}+J(\psi,v)=0, \tag{2.8}
$$

$$
\frac{\mathrm{D}\omega}{\mathrm{D}t}=\frac{\partial\omega}{\partial t}+J(\psi,\omega)=2\varepsilon h^4\left(J(\psi,v)-v\varepsilon\frac{\partial v}{\partial\phi}\right). \tag{2.9}
$$

It is clear that the quantity v is materially conserved. For the special case that v is piecewise constant, ω is also materially conserved except on boundaries. Note that v is non-zero outside the vortex to obtain appropriate decay at infinity, as will be discussed in Chapter 4.

Chapter 3

Inverting $\mathscr{L}\psi$

We have determined the quantity ω in terms of the helical stream function ψ. The following task is to invert the helical operator $\mathscr{L}\psi$. Through (2.6), the derivative of ψ respective to r and ϕ need to be computed to obtain the velocity field. [LUCAS & DRITSCHEL(2009)] provided a method to obtain the analytic solution: they decomposed ψ and ω as Fourier series in ϕ and found Green's functions for each mode. In this section, we invert $\mathscr{L}\psi$ by seeking the direct Green's function solution for (2.7).

With $G(r,\phi';r',\phi')$ the appropriate Green's function, we write the Green's function solution to (2.7) as

$$\psi = \int G\left(r,\phi';r',\phi'\right) F\left(r',\phi'\right) J(r',\phi')\mathrm{d}r'\mathrm{d}\phi'. \tag{3.1}$$

where $F(r,\phi) = \omega + 2\varepsilon h^4 v$ and the helical Jacobian $J(r,\phi) = rh$ which can be obtained from the gradient operator. The Green's function satisfies

$$\mathscr{L}G(r,\phi';r',\phi') = \frac{\delta(r-r')\delta(\phi-\phi')}{J(r,\phi)}. \tag{3.2}$$

Taking the source point to have coordinates r' and ϕ', using a discrete Fourier transform in the azimuthal direction ϕ leads to a decomposition of G in the form:

$$G(r,r';\phi,\phi') = \sum_m \hat{G}_m(r;r')e^{im(\phi-\phi')}.$$

Then (2.7) now leads to a set of ordinary differential equations for $m > 0$:

$$\hat{\mathscr{L}}_m \hat{G}_m = h\left[\frac{\mathrm{d}}{\mathrm{d}r}\left(rh^2\frac{\mathrm{d}}{\mathrm{d}r}\right) - \frac{m^2}{r}\right]\hat{G}_m = \delta(r-r'). \tag{3.3}$$

The modes with non-zero m satisfy:

$$\hat{\mathscr{L}}_m \hat{G}_m = h\left[\frac{r}{1+\varepsilon^2 r^2}G''_m + \frac{1-\varepsilon^2 r^2}{(1+\varepsilon^2 r^2)^2}G'_m - \frac{m^2}{r}G_m\right] = \delta(r-r'). \tag{3.4}$$

Introduce a new function $u(r)$ with $\hat{G}_m = ru$. Then we have the derivatives $\hat{G}'_m = ru' + u, \hat{G}''_m = ru'' + 2u'$. Then (3.4) becomes

$$r^2(1+\varepsilon^2 r^2)u'' + (3r + \varepsilon^2 r^3)u' + (1-\varepsilon^2 r^2)u - m^2(1+\varepsilon^2 r^2)^2 u = 0.$$

Change variable to $R = \varepsilon m r$, then we can write

$$R^2(m^2+R^2)u_{RR} + R(3m^2+R^2)u_R + (m^2-R^2)u - (m^2+R^2)^2 u = 0. \tag{3.5}$$

Recall that the modified Bessel function of order m with solutions $I_m(x)$ and $K_m(x)$ satisfy:

$$x^2 y'' + xy' - (x^2+m^2)y = 0.$$

Differentiating the equation with respect to x and multiplying by $m^2 + x^2$, we obtain

$$x^2(m^2+x^2)y''' + x(3m^2+x^2)y'' + (m^2-x^2)y' - (m^2+x^2)^2 y' = 0.$$

Comparing the equation to (3.5), we can obtain the solution for u as

$$u(r) = aI_m'(\varepsilon mr) + bK_m'(\varepsilon mr),$$

where the prime denotes the derivative respect to r and I_m and K_m are the modified Bessel functions of the first and second kind, of order m. Since $\hat{G}_m$ is bounded at origin and infinity, it can be shown that $\hat{G}_m$ has the form

$$\hat{G}_m(r;r') = A_0 \begin{cases} rI_m'(\varepsilon mr)\, K_m'(\varepsilon mr') & r < r', \\ rK_m'(\varepsilon mr) I_m'(\varepsilon mr') & r > r'. \end{cases} \tag{3.6}$$

where A_0 is a function of r', the term h' represents $h(r')$ and so on. The jump condition at $r = r'$ gives

$$h' \left[\left[rh^2 \frac{\partial}{\partial r} \hat{G}_m \right]\right] = 1. \tag{3.7}$$

Together with the relations for modified Bessel functions:

$$I_m''(r) = \frac{(r^2+m^2)I_m(r) - rI_m'(r)}{r^2}, \qquad K_m''(r) = \frac{(r^2+m^2)K_m(r) - rK_m'(r)}{r^2},$$
$$I_m'(r)K_m(r) - I_m(r)K_m'(r) = \frac{1}{r},$$

we can obtain

$$\begin{aligned} 1 &= r'h'^3 \cdot A_0 \varepsilon mr' \left[I_m'(\varepsilon mr')K_m''(\varepsilon mr') - I_m''(\varepsilon mr')K_m'(\varepsilon mr') \right] \\ &= r'h'^3 \cdot A_0 m \frac{1+\varepsilon^2 r'^2}{r'} \left[I_m(\varepsilon mr')K_m'(\varepsilon mr') - I_m'(\varepsilon mr')K_m(\varepsilon mr') \right] = A_0 \frac{h'}{\varepsilon r'}, \end{aligned}$$

which gives $A_0 = \varepsilon r'/h'$. We can now write (3.6) as

$$\hat{G}_m(r;r') = \begin{cases} \varepsilon \dfrac{rr'}{h'} I'_m(\varepsilon m r) K'_m(\varepsilon m r') & r < r', \\ \varepsilon \dfrac{rr'}{h'} K'_m(\varepsilon m r) I'_m(\varepsilon m r') & r > r'. \end{cases} \tag{3.8}$$

For the axisymmetric mode with $m = 0$, we can write

$$\hat{\mathscr{L}}_0 \hat{G}_0 = 2\pi h \left[\frac{\mathrm{d}}{\mathrm{d}r} \left(r h^2 \frac{\mathrm{d}\hat{G}_0}{\mathrm{d}r} \right) \right] = \delta(r - r'). \tag{3.9}$$

We have the coefficient 2π here since the integral of $\mathscr{L}G$ in space is unity. (3.9) can be solved directly to give:

$$\hat{G}_0(r;r') = \begin{cases} 0 & r < r', \\ \dfrac{1}{2\pi h'} \displaystyle\int_{r'}^{r} \frac{1}{r_0 h^2(r_0)} \mathrm{d}r_0 & r > r'. \end{cases} \tag{3.10}$$

Having derived each mode of the Green's function $G(r, r'; \phi, \phi')$, we can obtain the stream function ψ by inverting $\mathscr{L}\psi$ directly. We introduce the approach of [DRITSCHEL(1989)] in the next chapter, which requires the direct Green's function solution.

Chapter 4

Contour Dynamics

Consider the characteristic function f describing the material contour with $f > 0$ on the inside and $f < 0$ outside. Since f is materially conserved,

$$\frac{\mathrm{D}f}{\mathrm{D}t} = 0. \tag{4.1}$$

The quantity ω is materially conserved except on this boundary where a non-uniform vortex sheet develops in time. With a given initial vorticity inside the domain, we write

$$\omega = AH[f] + \Omega|\nabla f|\delta[f], \qquad v = CH[f] + v_\infty, \tag{4.2}$$

where A and C are materially conserved, Ω is the strength of the vortex sheet and H and δ are the Heviside and delta functions, respectively. For large r, the contribution from non-zero modes tends to zero, and we can write the axial velocity (2.3) in terms of the axisymmetric mode:

$$\begin{aligned}
\lim_{r\to\infty} u_z &= \lim_{r\to\infty} h^2\left(v_\infty+\varepsilon r\frac{\partial\psi}{\partial r}\right) = \lim_{r\to\infty} h^2\left(v+\varepsilon r\int\frac{\partial\hat{G}_0}{\partial r}F'r'h'\mathrm{d}'\phi'\right)\\
&= \lim_{r\to\infty} h^2\left[v_\infty+\varepsilon r\left(\int_V(A+2\varepsilon Ch'^4)\frac{\partial\hat{G}_0}{\partial r}r'h'\mathrm{d}r'\mathrm{d}\phi'+\oint\frac{\Omega r'}{2\pi rh^2}\mathrm{d}s'+4\varepsilon v_\infty\pi\int_0^\infty\frac{\partial\hat{G}_0}{\partial r}r'h'^5\mathrm{d}r'\right)\right]\\
&= \lim_{r\to\infty} h^2\left[v_\infty+\varepsilon rh\left(\frac{A}{2\pi rh^2}\int_V r'\mathrm{d}r'\mathrm{d}\phi'+2\varepsilon C\int_V\frac{\partial\hat{G}_0}{\partial r}r'h'^5\mathrm{d}r'\mathrm{d}\phi'+\frac{1}{2\pi rh^2}\oint\Omega r'\mathrm{d}s'+\varepsilon v_\infty r\right)\right]\\
&= \lim_{r\to\infty}\left[v_\infty+\frac{\varepsilon A}{2\pi}A_{\text{area}}+\frac{\varepsilon^2 C}{\pi}\int_V r'h'^4\mathrm{d}r'\mathrm{d}\phi'+\frac{\varepsilon}{2\pi}\oint\Omega r'\mathrm{d}s'\right],
\end{aligned}$$

where $A_{\text{area}}=\int_V r'\mathrm{d}r'\mathrm{d}\phi'$ is the area of the patch in r-ϕ plane. We want the axial velocity to vanish in this limit, and we can satisfy this constraint by setting

$$v_\infty=-\left[\frac{\varepsilon A}{2\pi}A_{\text{area}}+\frac{\varepsilon^2 C}{\pi}\int_V r'h'^4\mathrm{d}r'\mathrm{d}\phi'+\frac{\varepsilon}{2\pi}\oint\Omega r'\mathrm{d}s'\right], \tag{4.3}$$

a constant not necessarily equal zero. For the special case when C and Ω vanish, we find

$$v_\infty=-\frac{\varepsilon A}{2\pi}A_{\text{area}}. \tag{4.4}$$

In this case A_{area} is conserved. Considering both sides of (2.9), we have

$$\begin{aligned}
\frac{\mathrm{D}\omega}{\mathrm{D}t} = \frac{\mathrm{D}}{\mathrm{D}t}(AH[f]+\Omega\delta[f]|\nabla f|) &= A\delta[f]\frac{\mathrm{D}f}{\mathrm{D}t}+\delta[f]|\nabla f|\frac{\mathrm{D}\Omega}{\mathrm{D}t}+\Omega\delta[f]\frac{\mathrm{D}|\nabla f|}{\mathrm{D}t}+\Omega\delta'[f]|\nabla f|\frac{\mathrm{D}f}{\mathrm{D}t}\\
&= \delta[f]\left(\frac{\mathrm{D}\Omega}{\mathrm{D}t}|\nabla f|+\Omega\frac{\mathrm{D}|\nabla f|}{\mathrm{D}t}\right),\\
2\varepsilon h^4\left(J(\psi,v)-v\varepsilon\frac{\partial v}{\partial\phi}\right) &= 2\varepsilon h^4\left[C\delta[f]\frac{1}{r}(\frac{\partial\psi}{\partial r}\frac{\partial f}{\partial\phi}-\frac{\partial\psi}{\partial\phi}\frac{\partial f}{\partial r})-\frac{1}{2}\varepsilon\frac{\partial((CH[f]+v_\infty)^2}{\partial\phi}\right]\\
&= 2\varepsilon h^4\delta[f]\left[CJ(\psi,f)-\frac{1}{2}\varepsilon(C^2+2Cv_\infty)\frac{\partial f}{\partial\phi}\right].
\end{aligned}$$

Substituting into (2.9) leads to the governing equation for the vortex sheet strength in the form

$$\frac{\mathrm{D}\Omega}{\mathrm{D}t}|\nabla f| + \Omega\frac{\mathrm{D}|\nabla f|}{\mathrm{D}t} = 2\varepsilon h^4 \left[CJ(\psi, f) - \frac{1}{2}\varepsilon(C^2 + 2Cv_\infty)\frac{\partial f}{\partial \phi} \right]. \tag{4.5}$$

Let ξ be a parameter taken clockwise along the patch boundary in the (r,ϕ) plane and let $(r,\phi) = (R(\xi,t), \Phi(\xi,t))$ be the parametric representation of the boundary. Then the Lagrangian advection equations for the contour (R,Φ) in helical coordinates are

$$\frac{\partial R}{\partial t} = u_r(R,\Phi,t), \qquad \frac{\partial \Phi}{\partial t} = \frac{1}{Rh(R)} u_\phi(R,\Phi,t). \tag{4.6}$$

We have $Rh(R)$ here since

$$\frac{\mathrm{d}\boldsymbol{x}}{\mathrm{dt}} \cdot \boldsymbol{e}_\phi = rh\frac{\partial \phi}{\partial t}.$$

A schematic of parametrization is shown in figure 4.1.

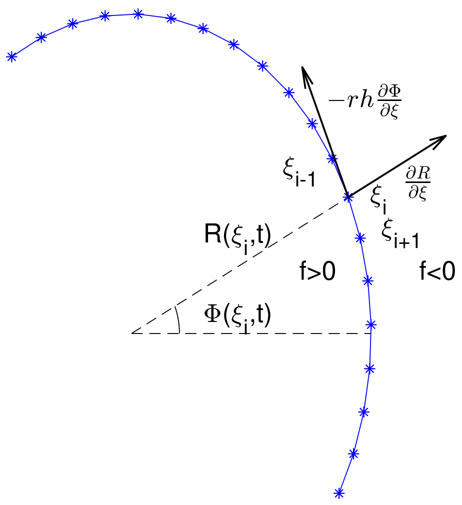

Figure 4.1: Schematic of parametrization $(R(\xi,t), \Phi(\xi,t))$. ξ is taken counter-clockwise along the patch boundary with $f < 0$ on the inside and $f > 0$ outside.

It follows from (4.1) that

$$\frac{1}{|\nabla f|}\frac{\mathrm{D}|\nabla f|}{\mathrm{D}t} = \frac{1}{L}\frac{\mathrm{D}L}{\mathrm{D}t} + \frac{u_r}{r}, \tag{4.7}$$

where

$$L^2(\xi,t) = |\nabla f|^2 = \left(Rh\frac{\partial\Phi}{\partial\xi}\right)^2 + \left(\frac{\partial R}{\partial\xi}\right)^2.$$

Consider Ω as a function of ξ and t, we have

$$\frac{\mathrm{D}\Omega}{\mathrm{D}t}|\nabla f| + \Omega\frac{\mathrm{D}|\nabla f|}{\mathrm{D}t} = L\left[\frac{\mathrm{D}\Omega}{\mathrm{D}t} + \Omega\left(\frac{1}{L}\frac{\mathrm{D}L}{\mathrm{D}t} + \frac{u_r}{r}\right)\right] = L\left[\frac{\partial\Omega}{\partial t} + \Omega\left(\frac{1}{L}\frac{\partial L}{\partial t} + \frac{1}{R}\frac{\partial R}{\partial t}\right)\right].$$

Then from the relations:

$$\frac{\partial f}{\partial r} = -rh\frac{\partial\Phi}{\partial\xi}, \qquad \frac{1}{rh}\frac{\partial f}{\partial\phi} = \frac{\partial R}{\partial\xi},$$

the governing equation (4.5) can be written as

$$\frac{\partial\Omega}{\partial t} + \Omega\left(\frac{1}{L}\frac{\partial L}{\partial t} + \frac{1}{R}\frac{\partial R}{\partial t}\right) = \frac{2\varepsilon h^5}{L}\left[C\left(\frac{1}{h}\frac{\partial R}{\partial\xi}u_\phi - R\frac{\partial\Phi}{\partial\xi}u_r\right) - \frac{1}{2}\varepsilon(C^2 + 2Cv_\infty)R\frac{\partial R}{\partial\xi}\right]. \tag{4.8}$$

Introduce $\gamma = \Omega LR$ simplifies (4.8) to

$$\frac{\partial\gamma}{\partial t} = 2\varepsilon h^5 R\left[C\left(\frac{1}{h}\frac{\partial R}{\partial\xi}u_\phi - R\frac{\partial\Phi}{\partial\xi}u_r\right) - \frac{1}{2}\varepsilon(C^2 + Cv_\infty)R\frac{\partial R}{\partial\xi}\right]. \tag{4.9}$$

When v is uniform and there is no vortex sheet on the boundary initially, we have $C = \gamma(0) = 0$. Through (4.9), we can deduce that there will be no vortex sheet generated at later times.

The approach of [Dritschel(1989)] is applied to to obtain a contour dynamics formulation. From (3.1), the vortex sheet part $F_s = \Omega|\nabla f|\delta(f)$ leads to the following contour integral for the stream function ψ:

$$\psi_s = \oint G(r,\phi;r'\phi')\Omega(r',\phi')r'h'\mathrm{d}s', \tag{4.10}$$

which can be differentiated directly to obtain the contribution of velocity.

To obtain the rest of the velocity field, we start with Green's theorem [DRITSCHEL(1989)] in the form

$$\int_V \left(\frac{1}{r'h'}\frac{\partial(r'h'Q)}{\partial r'} - \frac{1}{r'h'}\frac{\partial P}{\partial\phi'}\right) r'h'\mathrm{d}r'\mathrm{d}\phi' = \oint_C \left(P\mathrm{d}r' + r'h'Q\mathrm{d}\phi'\right), \tag{4.11}$$

Define new functions by

$$rh\frac{\partial P}{\partial\phi'} = r'h'\frac{\partial G}{\partial\phi}, \qquad \frac{1}{r'h'}\frac{\partial(r'h'Q)}{\partial r'} = \frac{1}{r'h'^5}\frac{\partial(r'h'S)}{\partial r} = \frac{\partial G}{\partial r}. \tag{4.12}$$

This gives

$$\begin{aligned}
P(r,\phi;r',\phi') &= -\frac{r'h'}{rh}\sum_{m\geq 0}\hat{G}_m(r;r')e^{im(\phi-\phi')},\\
Q(r,\phi;r',\phi') &= \frac{1}{r'h'}\sum_m\int\frac{\partial\hat{G}_m(r;r')}{\partial r}r'h'\mathrm{d}r'e^{im(\phi-\phi')},\\
S(r,\phi;r',\phi') &= \frac{1}{r'h'}\sum_m\int\frac{\partial\hat{G}_m(r;r')}{\partial r}r'h'^5\mathrm{d}r'e^{im(\phi-\phi')},
\end{aligned}$$

With (3.1), we can arrive at the equations for contour dynamics:

$$\begin{aligned}
\frac{\partial\psi_H}{\partial\phi} &= \int_V\frac{\partial G}{\partial\phi}(A+2\varepsilon h'^4C)r'h'\mathrm{d}r'\mathrm{d}\phi' + 2\varepsilon v_\infty\int_0^{2\pi}\int_0^\infty\frac{\partial G}{\partial\phi}r'h'^5\mathrm{d}r'\mathrm{d}\phi'\\
&= -rh\oint_C P(A+2\varepsilon h'^4C)\mathrm{d}r' + 2\varepsilon v_\infty\sum_m\int_0^{2\pi}\int_0^\infty \mathrm{i}m\hat{G}_m r'h'^5e^{im(\phi-\phi')}\mathrm{d}r'\mathrm{d}\phi'\\
&= -rh\oint_C P(A+2\varepsilon h'^4C)\mathrm{d}r',
\end{aligned} \tag{4.13}$$

$$
\begin{aligned}
\frac{\partial\psi_H}{\partial r} &= \int_V \left(A\frac{\partial G}{\partial r} + 2\varepsilon C \frac{\partial G}{\partial r} r' h'^4 \right) r' h' \mathrm{d}r' \mathrm{d}\phi' + 2\varepsilon v_\infty \int_0^{2\pi} \int_0^\infty \frac{\partial G}{\partial r} r' h'^5 \mathrm{d}r' \mathrm{d}\phi' \\
&= A \int_V \frac{\partial G}{\partial r} r' h' \mathrm{d}r' \mathrm{d}\phi' + 2\varepsilon C \int_V \frac{\partial G}{\partial r} r' h' h'^4 \mathrm{d}r' \mathrm{d}\phi' + 2\varepsilon v_\infty \sum_m \int_0^{2\pi} \int_0^\infty \frac{\partial \hat{G}_m}{\partial r} r' h'^5 e^{im(\phi-\phi')} \mathrm{d}r' \mathrm{d}\phi' \\
&= A \oint_C Q r' \mathrm{d}\phi' + 2\varepsilon C \oint_C S r' h' \mathrm{d}\phi' + \varepsilon v_\infty r.
\end{aligned}
\tag{4.14}
$$

Then from (2.6), the corresponding velocity components can be obtained as

$$
u_r(r,\phi,t) = -\frac{1}{r}\left(\frac{\partial\psi_s}{\partial\phi} + \frac{\partial\psi_H}{\partial\phi} \right), \qquad u_\phi(r,\phi,t) = h\left(\frac{\partial\psi_s}{\partial r} + \frac{\partial\psi_H}{\partial r} \right). \tag{4.15}
$$

These five equations, (4.6),(4.9) and (4.13-4.15), form a closed set of equations on the boundary.

Chapter 5

Stability analysis

In this section we perform a linear normal-modes stability analysis for a circular vortex patch with radius R_0. The perturbed boundary is $r = R_0 + \eta(\phi, t)$. To obtain the dynamic boundary conditions, [LUCAS & DRITSCHEL(2009)] allows the mean and the perturbed parts of the azimuthal velocity component to have a jump across the perturbed boundary $r = R + \eta$, and requires the full azimuthal component to be continuous. In this work, we assume that the pressure is continuous across the boundary. The dispersion relations obtained from the two different boundary conditions is the same.

5.1 Base flow

Start from the basic state with $\eta = 0$, so that ψ is only a function of r. We take v and ω to be piecewise constant inside and outside the patch, denoted by V_0, Ω_0 and $V_\infty, 0$. Then (2.7) can be written as

$$\begin{aligned} \mathscr{L}\Psi_1 &= \frac{1}{r}\frac{\mathrm{d}}{\mathrm{d}r}\left(rh^2\frac{\mathrm{d}\Psi_1}{\mathrm{d}r}\right) = \Omega_0 + 2\varepsilon h^4 V_0, \quad 0 < r < R_0, \\ \mathscr{L}\Psi_2 &= \frac{1}{r}\frac{\mathrm{d}}{\mathrm{d}r}\left(rh^2\frac{\mathrm{d}\Psi_2}{\mathrm{d}r}\right) = 2\varepsilon h^4 V_\infty, \quad r > R_0, \end{aligned} \tag{5.1}$$

which can be solved directly to give

$$\begin{aligned}\frac{\mathrm{d}\Psi_1}{\mathrm{d}r} &= \frac{\Omega_0 r}{2}(1+\varepsilon^2 r^2)+V_0\varepsilon r, \quad 0<r<R_0\\ \frac{\mathrm{d}\Psi_2}{\mathrm{d}r} &= \frac{c}{r}(1+\varepsilon^2 r^2)+V_\infty\varepsilon r, \quad r>R_0\end{aligned} \tag{5.2}$$

with $\mathrm{d}\Psi_1/\mathrm{d}r$ being bounded at the origin. In order for the axial momentum to remain bounded at infinity, zero axial velocity u_z is needed then, which gives

$$\lim_{r\to\infty} u_z = \lim_{r\to\infty} h^2\left(V_\infty+\varepsilon r\frac{\mathrm{d}\Psi_2}{\mathrm{d}r}\right) = \lim_{r\to\infty}(V_\infty+\varepsilon c)=0.$$

This leads to

$$\frac{\mathrm{d}\Psi_2}{\mathrm{d}r} = -\frac{V_\infty}{\varepsilon r}, \quad r>R_0.$$

In such case, $u_z=0$ is zero outside the vortex patch. We consider a basic state that there is no vortex sheet on the boundary, the continuity of u_θ and u_z across the boundary at $r=R_0$ are required, which leads to

$$V_0=V_\infty=-\frac{1}{2}\varepsilon\Omega_0 R_0^2. \tag{5.3}$$

Finally,

$$\begin{aligned}\frac{\mathrm{d}\Psi_1}{\mathrm{d}r} &= \frac{\Omega r}{2}(1+\varepsilon^2 r^2-\varepsilon^2 R_0^2), \quad 0<r<R_0\\ \frac{\mathrm{d}\Psi_2}{\mathrm{d}r} &= \frac{\Omega R_0^2}{2r}. \quad r>R_0\end{aligned} \tag{5.4}$$

5.2 Perturbed equation

Introduce perturbations with $\omega=\Omega_0(r)+\omega'$, $\psi_1=\Psi_1(r)+\psi_1'$, $\psi_2=\Psi_2(r)+\psi_2'$, $p=P(r)+p'$, where ψ_1 and ψ_2 denote the streams function inside and outside the patch. Then from

(2.7), (2.8) and (2.9), the corresponding linearized perturbed equations become

$$\frac{1}{r}\frac{\partial}{\partial r}\left(rh^2\frac{\partial \psi'}{\partial r}\right)+\frac{1}{r}\frac{\partial^2\psi'}{\partial \phi^2}=0, \tag{5.5}$$

$$\frac{\mathrm{D}v'}{\mathrm{D}t}=\frac{\partial v'}{\partial t}+\frac{1}{r}\left(\frac{\partial \psi}{\partial r}\frac{\partial v'}{\partial \phi}-\frac{\partial v'}{\partial r}\frac{\partial \psi}{\partial \phi}\right)=0, \tag{5.6}$$

$$\frac{\mathrm{D}\omega'}{\mathrm{D}t}=\frac{\partial \omega'}{\partial t}+\frac{1}{r}\left(\frac{\partial \psi}{\partial r}\frac{\partial \omega'}{\partial \phi}-\frac{\partial \omega'}{\partial r}\frac{\partial \psi}{\partial \phi}\right)=0, \tag{5.7}$$

Both ψ_1' and ψ_2' satisfy (5.5).

Consider the patch boundary described by $f=R_0+\eta(\phi,t)-r$. From the kinetic boundary condition (4.1), we can write

$$0=\frac{\partial \eta}{\partial t}+\frac{1}{r}\frac{\partial \psi}{\partial \phi}+\frac{1}{r}\frac{\partial \psi}{\partial r}\frac{\partial \eta}{\partial \phi}.$$

at $r=R_0+\eta$, valid both inside and outside the patch. Through linearization, the kinetic boundary conditions become

$$0=\frac{\partial \eta}{\partial t}+\frac{1}{r}\frac{\partial \psi_1'}{\partial \phi}+\frac{1}{r}\frac{\mathrm{d}\Psi_1}{\mathrm{d}r}\frac{\partial \eta}{\partial \phi}, \qquad 0=\frac{\partial \eta}{\partial t}+\frac{1}{r}\frac{\partial \psi_2'}{\partial \phi}+\frac{1}{r}\frac{\mathrm{d}\Psi_2}{\mathrm{d}r}\frac{\partial \eta}{\partial \phi}, \tag{5.8}$$

at $r=R_0$.

For the dynamic boundary condition, the momentum equation in azimuthal direction gives

$$\frac{\partial u_\phi}{\partial t}+u_r\frac{u_\phi}{\partial r}+\frac{u_\phi}{rh}\frac{\partial u_\phi}{\partial \phi}+\frac{u_\phi u_r}{r}=-\frac{1}{\rho rh}\frac{\partial p}{\partial \phi}.$$

Then, substituting with the helical velocity components from (2.6) leads to

$$h\frac{\partial^2\psi}{\partial t\partial r}-\frac{1}{r}\frac{\partial \psi}{\partial \phi}\frac{\partial}{\partial r}\left(h\frac{\partial \psi}{\partial r}\right)+\frac{h}{r}\frac{\partial \psi}{\partial r}\frac{\partial^2\psi}{\partial \phi\partial r}-\frac{h}{r}\frac{\partial \psi}{\partial \phi}\frac{\partial \psi}{\partial r}=-\frac{1}{\rho rh}\frac{\partial p}{\partial \phi}.$$

Since the pressure is continuous across the boundary, so is $\partial p/\partial\phi$. Then at the boundary $r=R_0$, we can obtain

$$\left[\left[h\frac{\partial^2\psi}{\partial t\partial r}-\frac{1}{r}\frac{\partial\psi}{\partial\phi}\frac{\partial}{\partial r}\left(h\frac{\partial\psi}{\partial r}\right)+\frac{h}{r}\frac{\partial\psi}{\partial r}\frac{\partial^2\psi}{\partial\phi\partial r}-\frac{h}{r^2}\frac{\partial\psi}{\partial\phi}\frac{\partial\psi}{\partial r}\right]\right]=0. \tag{5.9}$$

The linearized dynamic boundary conditions become

$$\begin{aligned} &h\frac{\partial^2\psi_1'}{\partial t\partial r}-\frac{1}{r}\frac{\partial\psi_1'}{\partial\phi}\frac{\partial}{\partial r}\left(h\frac{\mathrm{d}\Psi_1}{\mathrm{d}r}\right)+\frac{h}{r}\frac{\mathrm{d}\Psi_1}{\mathrm{d}r}\frac{\partial^2\psi_1'}{\partial\phi\partial r}-\frac{h}{r^2}\frac{\partial\psi_1'}{\partial\phi}\frac{\mathrm{d}\Psi_1}{\mathrm{d}r}\\ =&h\frac{\partial^2\psi_2'}{\partial t\partial r}-\frac{1}{r}\frac{\partial\psi_2'}{\partial\phi}\frac{\partial}{\partial r}\left(h\frac{\mathrm{d}\Psi_2}{\mathrm{d}r}\right)+\frac{h}{r}\frac{\mathrm{d}\Psi_2}{\mathrm{d}r}\frac{\partial^2\psi_2'}{\partial\phi\partial r}-\frac{h}{r^2}\frac{\partial\psi_2'}{\partial\phi}\frac{\mathrm{d}\Psi_2}{\mathrm{d}r}, \end{aligned} \tag{5.10}$$

at $r=R_0$.

5.3 Dispersion relation

Introduce normal modes with $[\omega',\psi_1',\psi_2',\eta]=[\hat{\omega}(r),\hat{\psi}_1(r),\hat{\psi}_2(r),\hat{\eta}(r)]e^{st+im\phi}$, where m is a non-negative integer. Note that here we actually mean $\eta=\mathrm{Re}\left(\hat{\eta}e^{st+im\phi}\right)$. Using temporal analysis with $s=s_R+\mathrm{i}s_I$, we obtain

$$\eta=|\hat{\eta}|e^{s_Rt}\cos\left(s_It+m\phi+\arg(\hat{\eta})\right).$$

When s_R is greater than zero, the flow has a positive growth rate and is unstable. For the case that s_R is equal or less than zero, the flow is neutrally stable or stable, respectively.

Starting from (5.5) for perturbed helical streamfunction leads to the following set of ordinary differential equation

$$\frac{1}{r}\frac{\mathrm{d}}{\mathrm{d}r}\left(rh^2\frac{\mathrm{d}\hat{\psi}}{\mathrm{d}r}\right)-\frac{m^2}{r}\hat{\psi}=0, \tag{5.11}$$

the homogeneous problem for (3.3). Hence we obtain

$$\hat{\psi} = B_1 r I_m'(\varepsilon m r) + B_2 r K_m'(\varepsilon m r).$$

for $m > 0$. To have $\hat{\psi}_{1,2}$ be bounded at $r = 0, \infty$, we require

$$\hat{\psi}_1 = B_1 r I_m'(\varepsilon m r), \quad \hat{\psi}_2 = B_2 r K_m'(\varepsilon m r), \tag{5.12}$$

where B_1 and B_2 are constant. The two boundary conditions (5.8) and (5.10) then lead to

$$B_2 K_m'(\alpha)\left(s + \frac{1}{R_0}\Psi_1'\right) = B_1 I_m'(\alpha)\left(s + \frac{1}{R_0}\Psi_2'\right), \tag{5.13}$$

$$B_1\left[\left(sh + \frac{\mathrm{i}mh}{R_0}\Psi_1'\right) I - \mathrm{i}m I_m' F_1\right] = B_2\left[\left(sh + \frac{\mathrm{i}mh}{R_0}\Psi_2'\right) K - \mathrm{i}m K_m' F_2\right]. \tag{5.14}$$

Here we write $F_{1,2} = h\left(h^2\Psi_{1,2}'/R_0 + \Psi_{1,2}''\right)$, $I = I_m' + \alpha I_m''$ and $K = K_m' + \alpha K_m''$ with $\alpha = \varepsilon m R_0$. We also write $I_m' = I_m'(\alpha)$ and so on. All the functions take values at $r = R_0$. Multiplying of (5.13) and (5.14) leads to the quadratic dispersion relations:

$$\begin{aligned} &-\frac{1}{\varepsilon^2 R_0^2 h}s^2 + s\frac{\mathrm{i}m}{R_0}\left[K_m'\Psi_1'\left(2hI - R_0 I_m' F_1\right) - I_m'\Psi_2'(2hK - R_0 K_m' F_2)\right] \\ &-\frac{m^2}{R_0^2}\left[K_m'\Psi_1'\left(h\Psi_1' I - R_0 I_m' F_1\right) - I_m'\Psi_2'\left(h\Psi_2' K - R_0 K_m' F_2\right)\right] = 0. \end{aligned} \tag{5.15}$$

We use the basic solution (5.4) when there is no vortex sheet on the patch boundary. Then (5.15) can be simplified to

$$\left(s + \frac{\mathrm{i}m\Omega_0}{2}\right)\left[-\frac{1}{\varepsilon^2 R_0^2 h}s + \frac{\mathrm{i}m\Omega_0}{R_0}\left(-\frac{1}{2\varepsilon^2 R_0 h} - \frac{R_0}{h}K_m'(\alpha) I_m'(\alpha)\right)\right] = 0. \tag{5.16}$$

Note that, the quadratic equation (5.15) holds for the case with vortex sheet as well. The solutions for (5.16) are

$$s = -\frac{\mathrm{i}m\Omega_0}{2}, \quad -\mathrm{i}m\Omega_0\left(\frac{1}{2} + \varepsilon^2 R_0^2 K_m'(\alpha) I_m'(\alpha)\right). \tag{5.17}$$

Note that $s = -\mathrm{i}m\Omega_0/2$ is not a valid solution: it solves (5.13) but it is not a solution for (5.14). Identifying the linear mode frequencies Ω_m [LUCAS & DRITSCHEL(2009)] with

$$\Omega_m = -\frac{s\mathrm{i}}{m\Omega_0} = -\left(\frac{1}{2} + \varepsilon^2 R_0^2 K_m'(\alpha) I_m'(\alpha)\right), \tag{5.18}$$

For $\alpha \ll 1$, these tend to the two-dimensional values $(m^{-1} - 1)/2$, while for $\alpha \gg 1$, they tend to the axisymmetric values $\varepsilon R_0/2m$ [SAFFMAN(1993)]. The solutions indicate that $\mathrm{Re}(s) = 0$ for all modes, R_0 and ε. This implies that the helical vortex patch is neutrally stable under linear instability analysis. However, the nonlinear evolution may lead to instability.

In this work, we only discuss the basic state that the vortex patch is centered at origin. When the patch is off center, obtaining the basic state is much more challenging. Such work will be done in further studies.

Chapter 6

Numerical calculations

We place $N = 128$ nodes on the boundary to represent the contour. We use Fourier series in terms of the parameter ξ to interpolate these nodes as

$$R(\xi) = \mathrm{Re}\left\{\sum_{|\mathrm{k}|=0}^{\mathrm{N}/2-1} \hat{\mathrm{R}}_{\mathrm{k}} \mathrm{e}^{\mathrm{i}\mathrm{k}\xi}\right\}, \qquad \Phi(\xi) = \mathrm{Re}\left\{\sum_{|\mathrm{k}|=0}^{\mathrm{N}/2-1} \hat{\Phi}_{\mathrm{k}} \mathrm{e}^{\mathrm{i}\mathrm{k}\xi}\right\}, \tag{6.1}$$

where $\hat{R}_k$ and $\hat{\Phi}_k$ are the Fourier transform of R and Φ, and ξ is equally spaced in $[0, 2\pi)$. The terms $\partial R/\partial\xi$ and $\partial\Phi/\partial\xi$ can be obtained directly by differentiating (6.1) with respect to ξ. We use the centroid position parameter (r_0, ϕ_0) to represent that we set the core of the vortex patch at $r = r_0$ and $\phi = \phi_0$ in r-ϕ plane initially. The initial circular contour is given by

$$R(\xi, 0) = \sqrt{R_0^2 + r_0^2 + 2R_0 r_0 \cos(\xi - \phi_0)}, \quad \Phi(\xi, 0) = \arctan\frac{R_0 \sin\xi + r_0 \sin\phi_0}{R_0 \cos\xi + r_0 \cos\phi_0}, \tag{6.2}$$

where R_0 is the patch radius and $\xi \in [0, 2\pi)$. Note that, for a certain patch in space, its contour in r-ϕ plane represents the projection of the patch on the x-y plane along the helical line which is shown in figure 6.1. For the ith node, we obtain $\partial R_i/\partial t$ and $\partial\Phi_i/\partial t$ from (4.6) and (4.13-4.15), $\partial\gamma_i/\partial t$ from (4.9). The contour integrals are computed using the trapezoidal rule. Then, R, Φ and γ are advanced in time using Fourth Order Runge-Kutta method with time step $\delta t = 0.05$ for

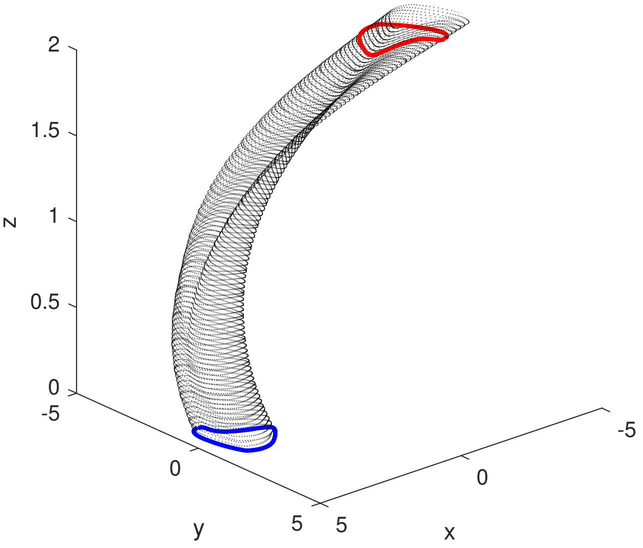

Figure 6.1: The higher bold curve represents the contour in three-dimensional space while the lower bold curve represents the contour in r-ϕ plane.

perturbed contour and $\delta t = 10^{-3}$ for shifted contour.

6.1 Perturbed contour

We perturb the initial contour given by the circular vortex patch centered at origin with different modes. The simulations are performed at a fixed value of the original patch radius $R_0 = 1$, with pitch $\varepsilon = 1.5$, vortex strength $A = 1$ and $C = 0$. Note that, C is the jump of v described in (4.2), and $C = 0$ corresponds to the case that there is no vortex sheet on the boundary. The strength of vortex sheet Ω has been set to zero initially, and we set $v_\infty = -1/2\varepsilon R_0^2$ to ensure that the velocity components are continuous across the boundary. Figure 6.2 and 6.3 show the time evolution of vortex patch in the r-ϕ plane when we give perturbation initially with $\eta_4(0) = 10^{-3}$ and $\eta_9(0) = 10^{-3}$. These two cases do not give the same evolution. For $\eta_4(0) = 10^{-3}$ (figure 6.2), the contour remains circular at short time ($t < 2.0$s), and deforms later ($t = 3.0, 4.0$s): 4

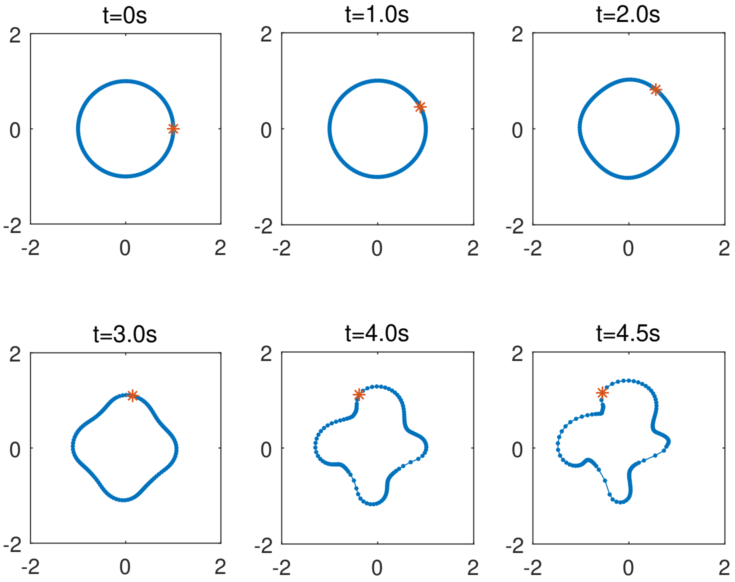

Figure 6.2: Contour evolution in r-ϕ plane with Initial mode amplitude $\eta_4(0) = 10^{-3}$. Star denotes the first node on the contour.

protrusions induced by initial perturbation have formed on the boundary like a quadrangular. The contour keeps deforming and the distribution of the nodes is no longer uniform ($t = 4.0, 5.0$s). In the evolution, the core of the vortex patch nearly remains at the origin. For the second case with $\eta_9(0) = 10^{-3}$ (figure 6.3), the contours remains circular for a longer time ($t < 3$s), and one half of the contour no longer have a smooth curvature later ($t = 4.5$s). Meanwhile, the core of the vortex patch has shifted. We stop the calculation when the contours get close to the origin to avoid the singularity.

To have a clearer view in space, we show the temporal evolution of the full three-dimensional helical vortex tube in figures 6.4 and 6.5. Each contour represents the horizontal cross-section of the vortex tube and all the contours for a certain instant are identical according to the helical symmetry. Note that the contours do not generally correspond to the same fluid particles for different instants since fluid particles do not have the same axial velocity while the contours are the horizontal cross-sections. Figure 6.4 describes the case that the initial mode

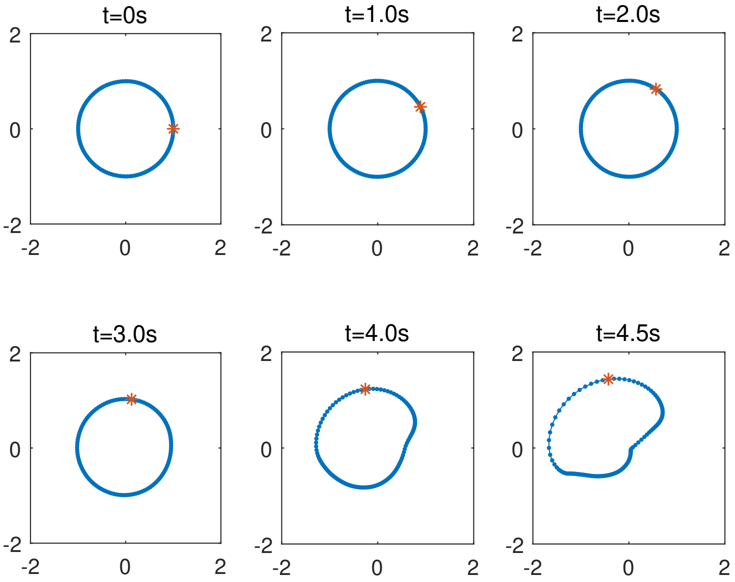

Figure 6.3: Contour evolution in r-ϕ plane with Initial mode amplitude $\eta_9(0) = 10^{-3}$. Star denotes the first node on the contour.

amplitude is $\eta_4(0) = 10^{-3}$. , The vortex tube remains cylindrical at the beginning ($t < 1.0$s) and becomes wavy later ($t = 2.0$s). Note that the cylindrical vortex tubes corresponds to the circular vortex patch centered at origin: all the cross sections have the same helical vectors $\boldsymbol{h}$. As the contours no longer remaining circular ($t > 3.0$s), the vortex tubes are deformed and twisted. When we perturbed initially with $\eta_9(0) = 10^{-3}$ (figure 6.5), the vortex tube become helical later ($t > 4.0$s) since the core of the patch is shifted.

Turning now to figure 6.6 and 6.7, we are able to observe the amplitude of each mode $\eta_m(t)$ at different instants from the mode spectrum. Note that the amplitudes have been normalized to the original radius R_0. For the first case with $\eta_4(0) = 10^{-3}$ (figure 6.6), contrary to what we are expecting in the linear temporal analysis, $\eta_1(t)$ grows with time. The contour is dominated by the 4th mode initially ($t < 3.0s$) and led to the quadrangular like deformation. The first mode grows rapidly and has higher amplitude later. For the case with $\eta_9(0) = 10^{-3}$ (figure 6.7), the mode spectrum has a different trend as time increases: the amplitude of the 9th mode remains

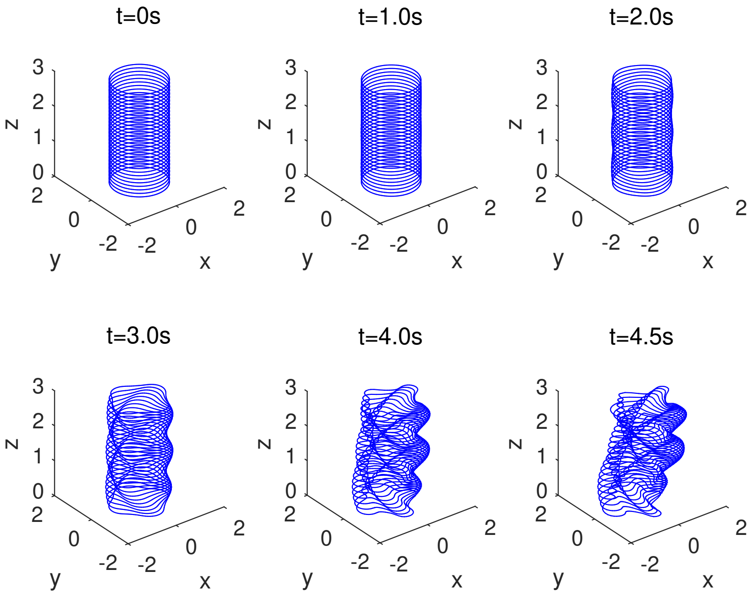

Figure 6.4: Shown are the evolution of the helical vortex tube with the full three-dimensional with Initial mode amplitude $\eta_4(0) = 10^{-3}$, viewed from a perspective of 30° elevation. Each contour denotes the horizontal cross-section of the vortex tube.

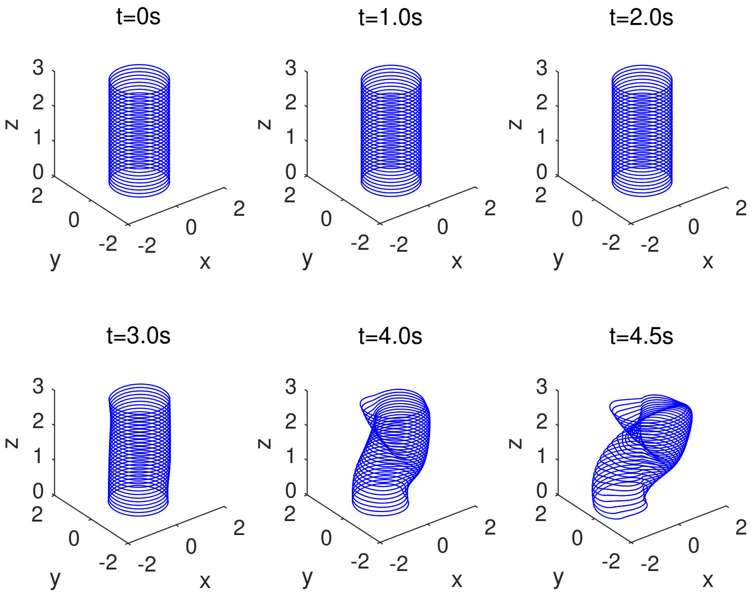

Figure 6.5: Shown are the evolution of the helical vortex tube with the full three-dimensional with Initial mode amplitude $\eta_9(0) = 10^{-3}$, viewed from a perspective of 30° elevation. Each contour denotes the horizontal cross-section of the vortex tube.

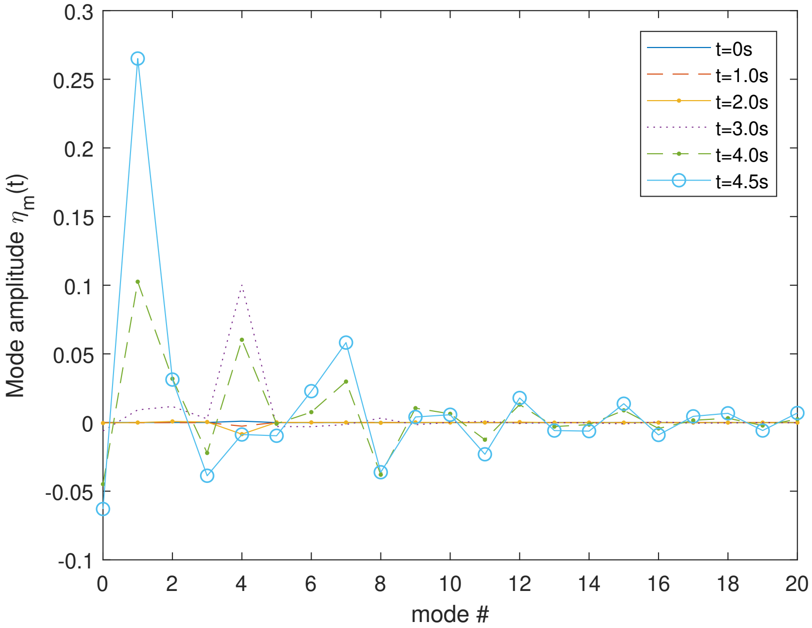

Figure 6.6: Shown are the mode spectrum for different instants with initial mode amplitude $\eta_4(0) = 10^{-3}$.

at a low level and the 1st mode grows significantly and dominates at later times. In this case, rather than the 9th mode, the 1st mode becomes the most unstable mode. These results imply that nonlinear terms need to be considered in further studies to investigate the instability of the helical vortex patch.

When there is no vortex sheet generated on the boundary, as in (4.4), we expect the area of the patch in the r-ϕ plane to be conserved. Figure 6.8 shows the evolution of the normalized patch area. For both the two cases, the normalized areas remain at unity initially $(t < 2.5s)$ and grow rapidly later $(t > 4s)$. The areas are not conserved since the error from numerical process is accumulated.

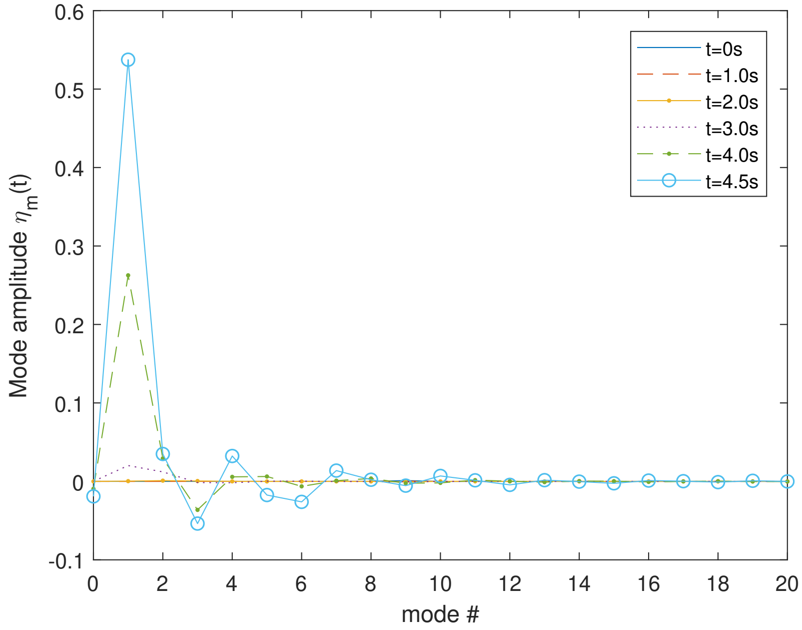

Figure 6.7: Shown are the mode spectrum for different instants with initial mode amplitude $\eta_9(0) = 10^{-3}$.

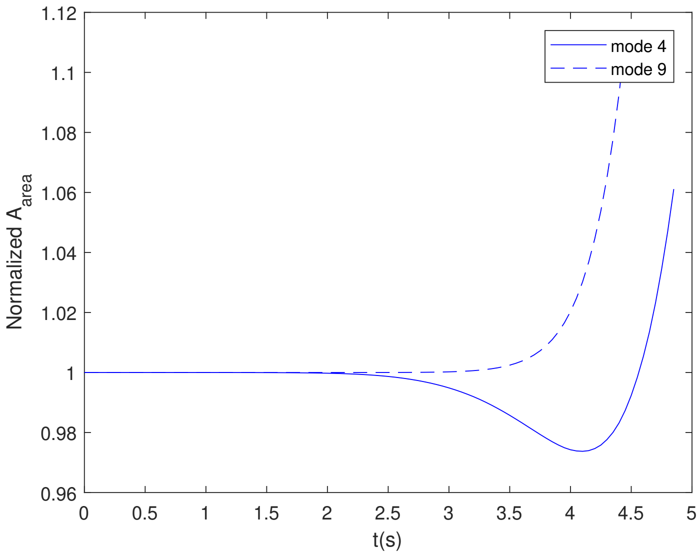

Figure 6.8: Curves shown are evolution of the patch areas. The areas have been normalized by the initial areas.

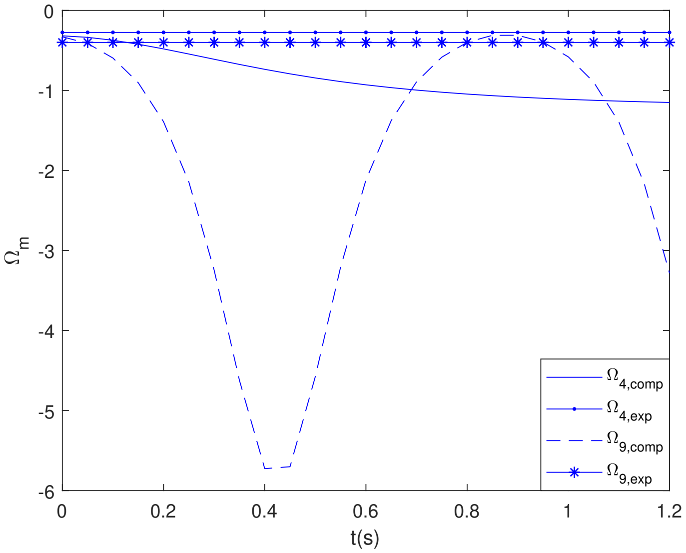

Figure 6.9: Curves showing the evolutions of the rotation rate computed from the evolution process ($\Omega_{4,9,\mathrm{comp}}$) and the expected analytic linear mode frequencies ($\Omega_{4,9,\mathrm{exp}}$) of a perturbed helical symmetric vortex. The expected values are $\Omega_4 = -0.2750$ and $\Omega_9 = -0.3999$ obtained from (5.18) when we take $m = 4$ and 9.

From (5.18), the angular frequencies of the linear helical modes are $\Omega_4 = -0.2750$ and $\Omega_9 = -0.3999$. Figure 6.9 shows Ω_4 and Ω_9 versus the rotation rate Ω_m computed from the evolution process. Initially, the computed $\Omega_{4,\mathrm{comp}}$ and $\Omega_{9,\mathrm{comp}}$ are quite close to the expected values and decay rapidly in a short time. The computed $\Omega_{4,\mathrm{comp}}$ decays slowly while the computed $\Omega_{9,\mathrm{comp}}$ decays rapidly in a short time and oscillates.

6.2 Shifted contour

Having examined parameter space in the case of vortex patch centered at origin, we extend the method to the shifted circular patch. When performing the simulation, we fix the value of the vortex strength $A = 1$, pitch $\varepsilon = 1.5$ and the initial strength of vortex sheet $\Omega_0 = 0$. For different original patch radii R_0, we set $v_\infty = -1/2\varepsilon R_0^2 - \varepsilon^2 C/\pi \int_V r' h'^4 \mathrm{d}r' \mathrm{d}\phi'$.

First, we consider the case with $C = 0$, which means no vortex sheet will be generated

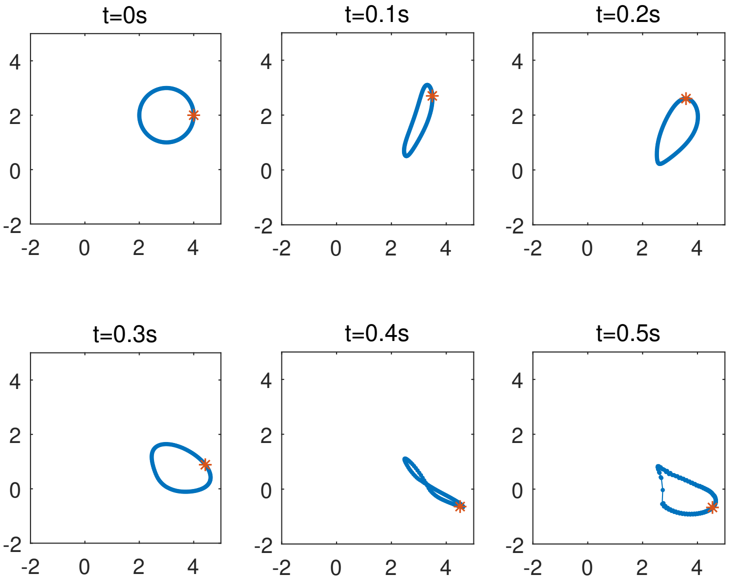

Figure 6.10: Contour evolution in r-ϕ plane with $(r_0, \phi_0) = (\sqrt{13}, \arctan(2/3)), R_0 = 1, C = 0$. Star denotes the first node on the contour.

on the boundary at the later times. Figure 6.10 describes the time evolution of vortex patch in r-ϕ plane. The vortex patches are twisted and flipped around. The contour crosses itself at $t = 0.4s$. The whole vortex patch is moving clockwise. We show evolution of the contours along with the full three-dimensional helical vortex in figure 6.11. At $t = 0$, the contours represent the horizontal cross-section of the vortex tube while each contour contains the same fluid particles for different instants. Contrary to the case that the contour centered at the origin, the vortex tube for the shifted contour is already helical in three-dimension initially.

When taking the vortex sheet into account, figure 6.12 and 6.13 shows the time evolution of vortex patch with $C = 20$ in r-ϕ plane. Two cases have been considered in this figure: the circular patch with centroid position parameter $(r_0, \phi_0) = (\sqrt{13}, \arctan(2/3))$ and patch radius $R_0 = 1.0$ (figure 6.12) and the circular patch with centroid position parameter $(r_0, \phi_0) = (3, 0)$ and $R_0 = 0.8$ (figure 6.13). With higher shifted radius r_0 and patch radius R_0, the contour in first case has a higher rotation rate in the first case. Compared to the case without vortex sheet, the

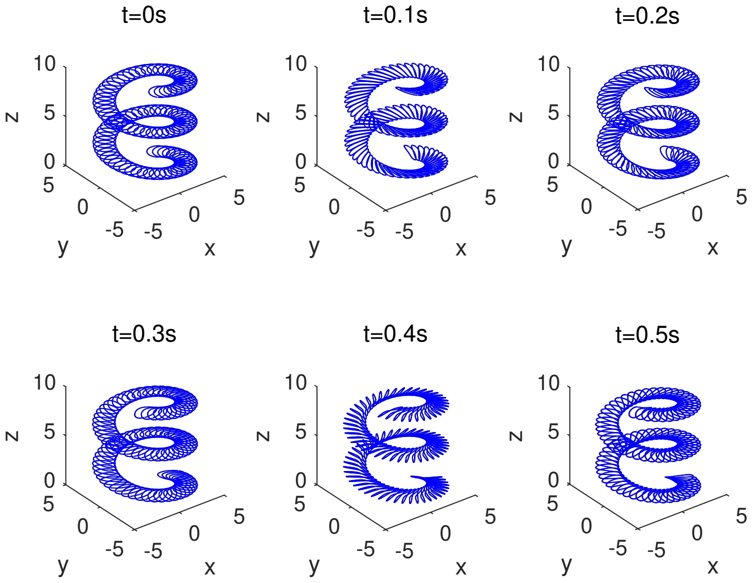

Figure 6.11: Shown are the evolution of the contours for $(r_0, \phi_0) = (\sqrt{13}, \arctan(2/3)), R_0 = 1, C = 0$ along with the full three-dimensional helical vortex tube, viewed from a perspective of 30° elevation. At $t = 0$, the contours are the horizontal cross section of the vortex tube.

effect of adding a vortex sheet on the contour boundary is to accelerate the process twisting and rotating the patch. The distribution of the nodes for the second case is not uniform in the later time. For some instants, the contours in r-ϕ plane may cross themselves since the fluid particles on the contours do not generally have the some velocity components in the helical direction $\boldsymbol{h}$ and then the contours will evolve in space.

We show the time evolution of the contours along with the full three-dimensional helical vortex tube in figure 6.14 and 6.15. The contours represent the horizontal cross section of the vortex tube at $t = 0$. The contours are flipping in space and this deformation leads to the crossing in r-ϕ plane.

Figure 6.16 and6.17 show the evolution of the vortex sheet strength Ω. In this figure, $\tilde{l}$ denotes distance for each node along the sheet normalized by its total length; $\tilde{l} = 0$ always corresponds to the first node and $\tilde{l} = 1$ coincides with $\tilde{l} = 0$. Note that the same value of $\tilde{l}$ does not generally correspond to the same fluid particle for different instants since the distance between

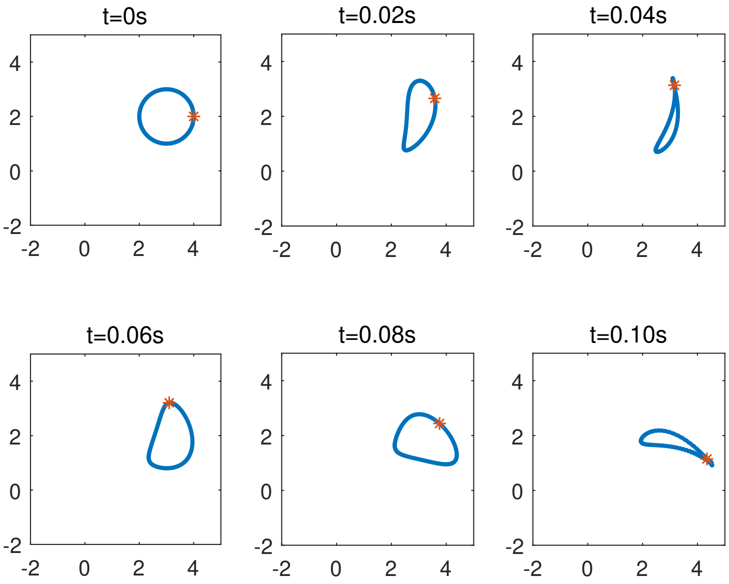

Figure 6.12: Contour evolution in r-ϕ plane with $(r_0, \phi_0) = (\sqrt{13}, \arctan(2/3)), R_0 = 1, C = 20$. Star denotes the first node on the contour.

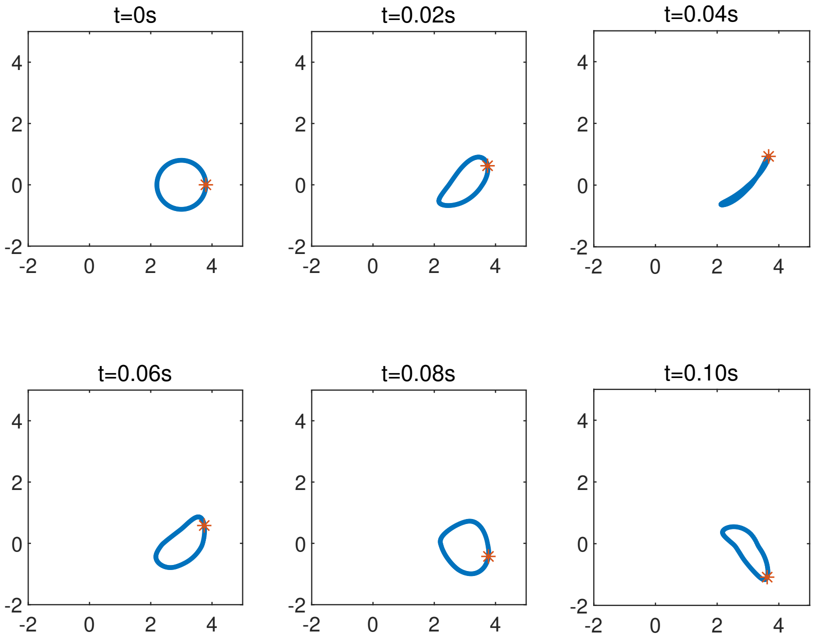

Figure 6.13: Contour evolution in r-ϕ plane with $(r_0, \phi_0) = (3, 0), R_0 = 0.8, C = 20$. Star denotes the first node on the contour.

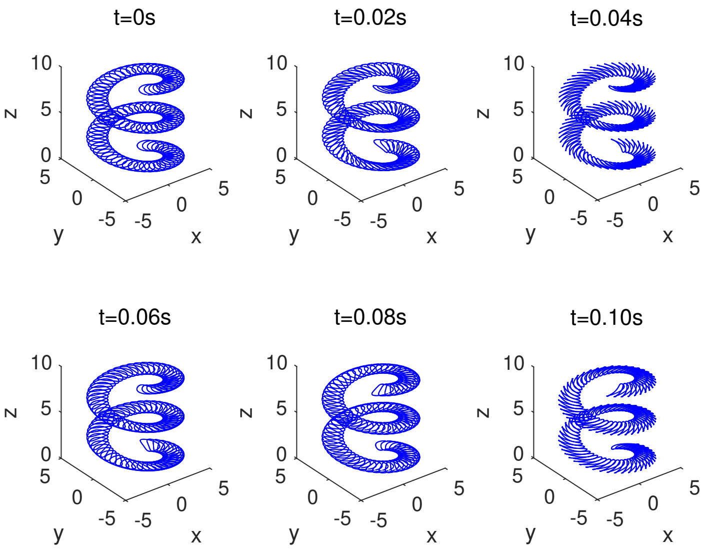

Figure 6.14: Shown are the evolution of the contours for $(r_0, \phi_0) = (\sqrt{13}, \arctan(2/3)), R_0 = 1, C = 20$ along with the full three-dimensional helical vortex tube, viewed from a perspective of 30° elevation. At $t = 0$, the contours are the horizontal cross section of the vortex tube.

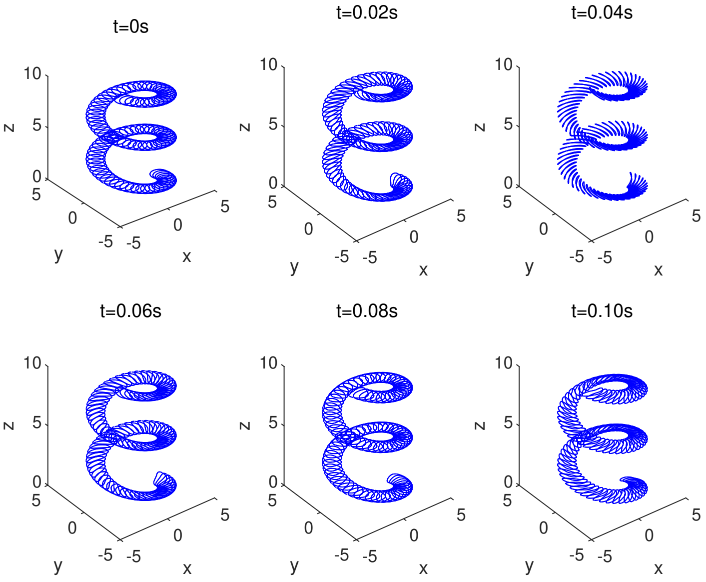

Figure 6.15: Shown are the evolution of the contours for $C = 20, (r_0, \phi_0) = (3, 0), R_0 = 0.8, C = 20$ along with the full three-dimensional helical vortex tube, viewed from a perspective of 30° elevation. At $t = 0$, the contours are the horizontal cross section of the vortex tube.

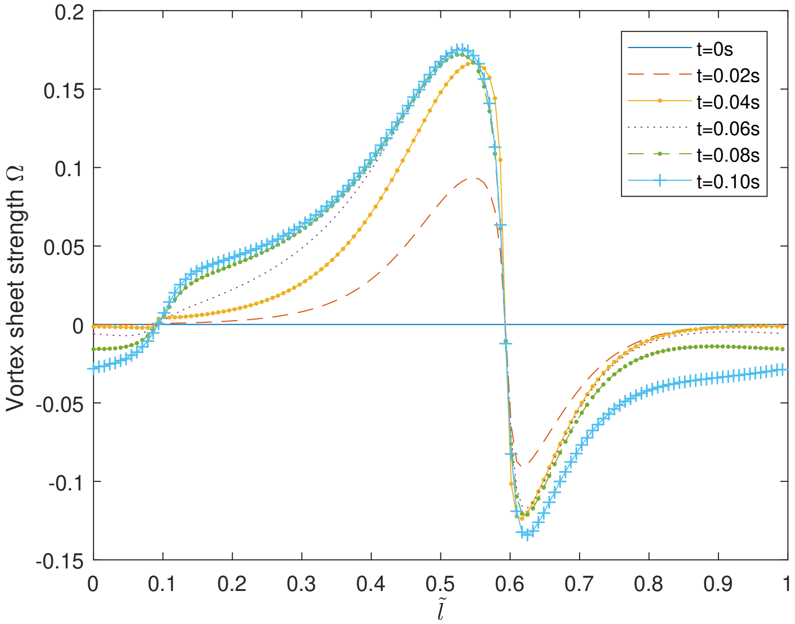

Figure 6.16: Strength of vortex sheet Ω as a function of normalized length $\tilde{l}$ for $(r_0, \phi_0) = (\sqrt{13}, \arctan(2/3)), R_0 = 1, C = 20$.

successive nodes changes with time. In each case, the sheet strength remains zero at two specific values of the normalized length: $\tilde{l} = 0.1, 0.6$ in figure 6.16 and $\tilde{l} = 0, 0.5$ in figure 6.17. The sheet strength and the difference across the $\tilde{l}$ axis generally increase with time. The sharpen shocks of the vortex sheet strength Ω are generated for both cases and leads to the discontinuity. Separated by the sharpen shock, Ω behaves oppositely like a shifted odd function.

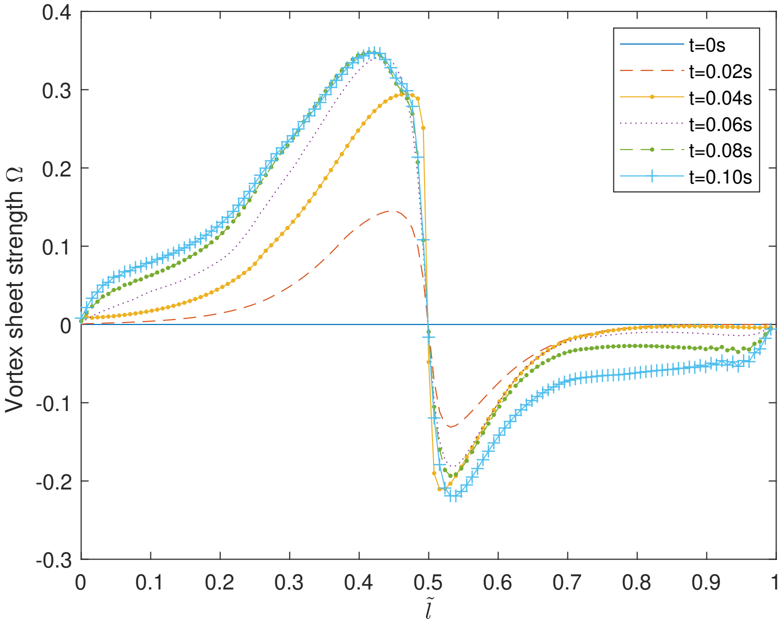

Figure 6.17: Strength of vortex sheet Ω as a function of normalized length $\tilde{l}$ for $C = 20, (r_0, \phi_0) = (3, 0), R_0 = 0.8, C = 20$.

Chapter 7

Conclusion

This paper has presented an analytic method for computing contour dynamics formulations for helically symmetric vortices. Fourier transforms were employed to invert the linear operator $\mathscr{L}\psi$ for axial vorticity and Green's theorem in helical coordinates was applied to obtain the contour integral for the stream function ψ. One can obtain the inversion relation linking vortex patch and sheet strength to velocity to compute the motion, (3.1), (4.13) and (4.14), and evolution equation for the vortex sheet strength (4.9).

We apply a temporal linear instability analysis for a piecewise constant distribution of axial vorticity. It turns out that this kind of vortex patch is neutrally stable to the infinitesimal perturbations. The linear mode frequencies Ω_m are shown in (5.18).

The contours we presented are parametrized by pitch ε, mean core radius R_0, centroid position (r_0, ϕ_0), axial vorticity A and initial velocity jump across the boundary C. Small ε shows two-dimensional flow while large ε recovers the axisymmetric case.

First we computed the evolution described by contours bounding regions of unity axial vorticity. We presented two different cases for perturbed contours, both of them showed unstable features. When we give perturbation with $\eta_4(0)$ and $\eta_9(0)$, we can inspect the feature induced by the mode 4 while the amplitude of mode 9 remains at a low level at all time. The first mode always becomes the most unstable mode at later times. This implies that the modes are coupled in the evolution and nonliear theory need to be applied.

For the shifted contours, we added the vortex sheet around the boundary. The numerical simulations of the evolution of vortex sheets were performed and shown in (6.16) and (6.17). Adding the vortex sheet on the boundary of the shifted contour accelerated the twisting and rotating process. In the distribution of Ω, sharpening shocks were generated for both cases. This leads to the discontinuity of Ω in the later time.

Chapter 8

Future Work

One of the very first steps in the future is to consider the non-linear relation in instability analysis. From the results for perturbed contours, they do not follow what we expected in linear stability analysis. The modes couple with each other which implies that the non-linear term need to be investigated in further studies. Meanwhile, obtaining the basic state for off center contours will help us to study the stability for such contours.

The next step would be to evaluate integrals with singularities in complicated domains. In our case, T]the calculation becomes complicated when the contours get close to the origin by the existence of singularities. For the evaluation of layer potentials, the method: Quadrature by Expansion [A.KLÖCKNER & O'NEIL(2013)] might be helpful.

The thesis is currently being prepared for submission for publication of the material. Tianyi Chu, Stefan G. Llewellyn Smith and Ching Chang. The thesis author was the primary investigator and author of this material.

Bibliography

[A.Klöckner & O'Neil(2013)] A.KLÖCKNER, A. BARNETT, L. GREENGARD & O'NEIL, M. 2013 Quadrature by expansion: A new method for the evaluation of layer potentials. *J. Comput. Phys.* **252**, 332–349.

[C.Selçuk(2017)] C.SELÇUK, I.DELBENDE, AND M.ROSSI 2017 Helical vortices: Quasiequilibrium states and their time evolution. *Physical Review Fluids* **2**.

[Delbende(2012)] DELBENDE, IVAN 2012 Direct numerical simulation of helical vortices. *Int. J. Engineering Systems Modelling and Simulation.* **4**, 94–101.

[Dritschel(1989)] DRITSCHEL, D.G. 1989 Contour dynamics and contour surgery: Numerical algorithms for extended, high-resolution modelling of vortex dynamics in two-dimensional, inviscid, incompressible flows. *Comput. Phys. Rep.* **10**, 77–146.

[Dritschel(1991)] DRITSCHEL, D.G. 1991 Generalized helical beltrami flows in hydrodynamics and magnetohydrodynamics. *J. Fluid Mech.* **222**, 525–541.

[Hattori & Fukumoto(2014)] HATTORI, YUJI & FUKUMOTO, YASUHIDE 2014 Modal stability analysis of a helical vortex tube with axial flow. *J. Fluid Mech.* **738**, 222–249.

[Lucas & Dritschel(2009)] LUCAS, DAN & DRITSCHEL, D.G. 2009 A family of helically symmetric vortex equilibria. *J. Fluid Mech.* **634**, 245–268.

[Saffman(1993)] SAFFMAN, P. G. 1993 *Vortex Dynamics*. Cambridge University Press.

[S.V. Alekseenko & S.I.Shtork(1999)] S.V. ALEKSEENKO, P.A. KUIBIN, V.L.OKULOV & S.I.SHTORK 1999 Helical vortices in swirl flow. *J. Fluid Mech.* **382**, 195–243.

[Widnall(1972)] WIDNALL, SHEILA E. 1972 The stability of a helical vortex filament. *J. Fluid Mech.* **54**, 641–663.